ACS APPLIED MATERIALS & INTERFACES

Research Article

www.acsami.org

ZnO Electron Field Emitters on Three-Dimensional Patterned Carbon Nanotube Framework

Chen Li, Chi Li, Yunsong Di, Wei Lei, Jing Chen,* and Yunkang Cui

School of Electronic Science and Engineering, Southeast University, Nanjing 210096, China

ABSTRACT: A three-dimensional patterned CNT framework was prepared in a thermal chemical vapor deposition system. ZnO nanoneedles with different areal density were subsequently grown on it via hydrothermal method. By combining the advantages of high aspect ratio, more effective emission sites with minimized screen effect and good Ohmic contact between ZnO nanoneedles and CNT framework, the ZnO/CNT hierarchical nanostructures with medium areal density exhibit a favorable FE performance which makes it promising candidate for cold cathode nanomaterials.

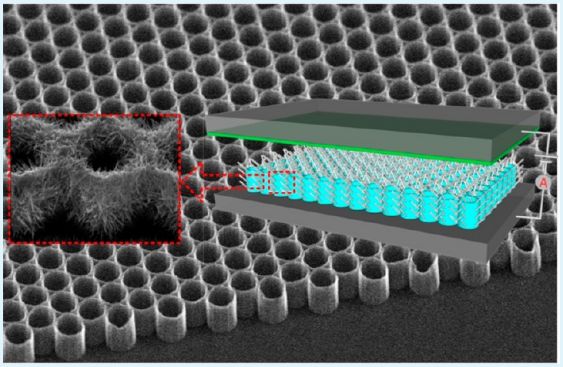

KEYWORDS: *ZnO, canbon nanotube, field emission, three-dimensional, hydrothermal, screening effect*

INTRODUCTION

In recent years, intensive efforts have been devoted to fabricate cold cathode field emitters with large current density and reliable performance because of their potential applications such as flat panel field emission displays (FED),[1] microwave power amplifier tubes,[2] and X-ray generators.[3] One-dimensional (1D) nanotubes[4] and two-dimensional (2D) nanosheets[5] are the most common field emitters and have been considered as important cold cathode nanomaterials for field emission (FE). In order to further optimize the FE performance, three-dimensional (3D) nanostructures such as complex carbon nanoneedles,[6] urchin-like ZnO nanostructures,[7] tungsten oxide nanowire network[8] and urchin-like α-Fe_2O_3 microstructure[9] have also been fabricated. These nanostructures are composed of long and sharp needles pointing in various directions, and it is believed to be favorable for enhancing the FE current density. Among these cold cathode nanomatericals, carbon nanotubes (CNTs) have been attracted the most attention for their excellent physical and chemical properties. However, many researchers have found that the breakdown of CNTs induced by Joule heating under high vacuum conditions could leads to the FE instability during the emission process.[10,11] In the meanwhile, ZnO semiconductor with a direct wide bandgap (3.37 eV) and large exciton binding energy (60 meV) also exhibits comparable FE property with that of carbon based nanostructures. And as an oxide material, high thermal stability and oxidation resistance also make ZnO stable field emitters in harsh vacuum environments.

By combining the merits of ZnO and carbon based nanostructures, ZnO/CNT hybrids were utilized as field emitters in recent works. Sugavaneshwar et al. reported the synthesis of ZnO nanotips on a multi-walled CNT mat and achieved a low threshold voltage of 1.5 V/μm.[12] Ho et al. believed that a direct coating of ZnO nanoparticles on CNTs reduced the defects or impurities on the CNT walls which optimized the conductivity.[13,14] Ding et al. also reported the growth of ZnO nanowires field emitters on CNT mesh array in a chemical vapor deposition (CVD) system and their FE properties.[15] Although these works showed good FE performances, the controllable large-scale growth of ZnO/CNT hierarchical nanostructures with high aspect ratio and minimized screening effect remains to be a challenge. ZnO nanostructures and CNTs are usually entangled together or randomly oriented, resulting in a serious screen effect which could depress the electric field on the emission sites.

Here, we report the synthesis and FE performance of ZnO nanoneedle field emitters on three-dimensional patterned CNT framework. Comparing with the conventional two-dimensional planar field emitters, the hierarchical ZnO/CNT nanostructures take the advantages of high aspect ratio, increased effective emission sites, and controllable screening effect. They are expected to be a candidate for the cold cathode nanomaterials.

EXPERIMENTAL SECTION

The ZnO/CNT hierarchical nanostructures were fabricated by a two step growth process. Silicon substrate was ultrasonically cleaned by deionized (DI) water, acetone, and isopropyl alcohol consecutively, then dried at 100 °C in an oven. Molybdenum (Mo) electrode of 1 μm wide was patterned by photolithography with periodic circular shapes. Two layers of aluminum (10 nm)/iron (1 nm) catalyst film were deposited on the electrode by sputtering technique. Then, the CNT framework is synthesized at 450°C for 60 seconds in a thermal

Received: July 9, 2013
Accepted: August 20, 2013
Published: August 20, 2013

CVD system (Black Magic, AIXTRON). The growth processes were described in detail with our previous work.[16] ZnO nanoneedles were subsequently synthesized on the CNT framework by hydrothermal method. A ZnO seed layer was deposited on the surface of CNT framework and the substrate by ultrasonic spraying pyrolysis for 5 mins. The hydrothermal reaction solution was prepared by mixing 0.01 M zinc nitrate (99.9%, Aldrich) and 0.01 M hexamethylenetetramine (99%, Aldrich) solution to adjust the pH value to 10.35 in an autoclavable screw cap bottle. Three substrates were then immersed into the reaction solution and heated at 95 °C for 10, 14, and 18 h, respectively. Eventually, the color of as-grown samples changed from black to gray.

The structure and morphology of the samples were characterized by scanning electron microscope (SEM, FEI Quanta 200F). The FE performance of current density versus electric field was carried out with a parallel-plate diode configuration in a vacuum chamber. The pressure in the chamber was maintained with 1.0×10^{-6} Torr at room temperature. A Teflon film with an aperture of 2 mm^2 was used as a spacer and inserted between the anode and cathode. The emission current was recorded with a Keithley $I-V$ meter by varying the applied anode voltage.

RESULTS AND DISCUSSION

The typical SEM image of the as-prepared CNT framework was shown in Figure 1a. The 10 μm high CNT forests were

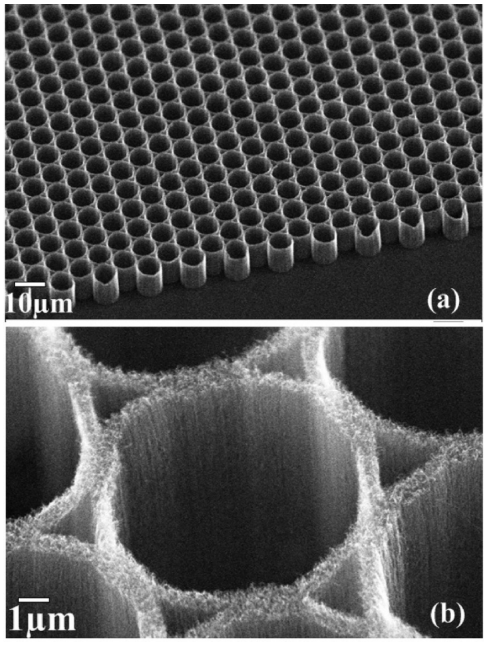

Figure 1. SEM images of as-prepared CNT framework under (a) low and (b) high magnification, respectively.

vertically aligned and densely grown on the substrate to form a well-defined framework. The three-dimensional framework was consisted by interconnected circular microchannels with a diameter of 8 μm. The detail of one single mircochannel in the framework is clearly evident in Figure 1b. The microchannels were surrounded by CNT forests of 1 μm thick, which is consistent with the width of the Mo electrode.

Figure 2a exhibits the SEM image of ZnO nanoneedles hydrothermally grown on the three-dimensional CNT framework with 14 h under low magnification. Figure 2b–d represent the high magnification SEM images of as-prepared ZnO/CNT hierarchical nanostructures grown with 10 (sample A), 14 (sample B), and 18 h (sample C), respectively. It is obvious

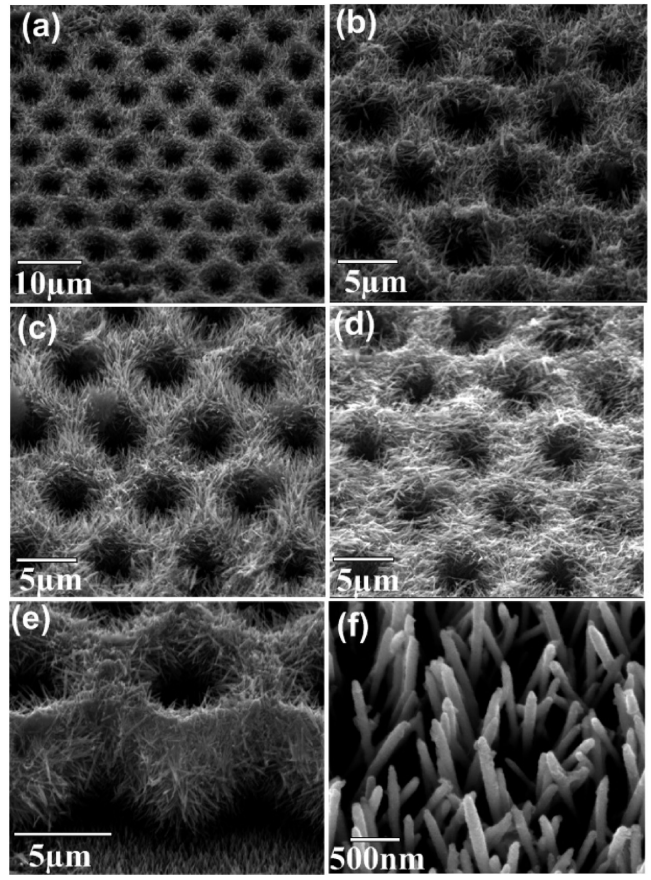

Figure 2. (a) SEM images of ZnO nanoneedles hydrothermally grown on the three-dimensional CNT framework with 14 h under low magnification. SEM images of ZnO/CNT hierarchical nanostructures with (b) 10, (c) 14, and (d) 18 h under high magnification, respectively. (e) Enlarged SEM images of one single ZnO/CNT hierarchical nanostructure and (f) the ZnO nanoneedles in sample B, respectively.

that the surface of CNT framework was densely covered by ZnO nanoneedles. As the growth time extended, the length of ZnO nanoneedles increased to ~3 μm and diminished the space in the microchannels. Figure 2e and f represent the enlarged SEM images of one single ZnO/CNT hierarchical nanostructure and the ZnO nanoneedles in sample B, respectively. The ZnO nanoneedles with a diameter of ~100 nm were grown on the grids and sidewalls of the CNT framework. Owing to the vertically aligned CNT forests, their three-dimensional circular microchannels provide more surface area to grow ZnO nanoneedles without consuming extra substrate space. The microchannels in the CNT framework uphold the ZnO field emitters to obtain a high aspect ratio and also separate the field emitters with their hollow microchannels to minimize the screening effect. Therefore, it is possible for the ZnO/CNT hierarchical nanostructures to obtain a high electric field at their FE tips which is essential for an enhanced FE current.

The FE performances can be evaluated by the simplified Fowler–Nordheim (F–N) equation $J = A(\beta^2E^2/\varphi)\exp(-B\varphi^{3/2}/\beta E)$, which describes the tunneling of electrons through a metal-vacuum barrier.[17] In the equation, J is the current density, A and B are constants with values of $A = 1.56 \times 10^{-10}$ (AV^{-2} eV) and $B = 6.83 \times 10^3$ (V $eV^{-3/2}$ μm^{-1}), respectively. β is a field enhancement factor which quantifies

dx.doi.org/10.1021/am402709r | ACS Appl. Mater. Interfaces 2013, 5, 9194–9198

the geometrical parameter of the field emitters, φ is the work function of the field emitter, and E is the applied electric field. Figure 3a shows the measured FE current density as a function

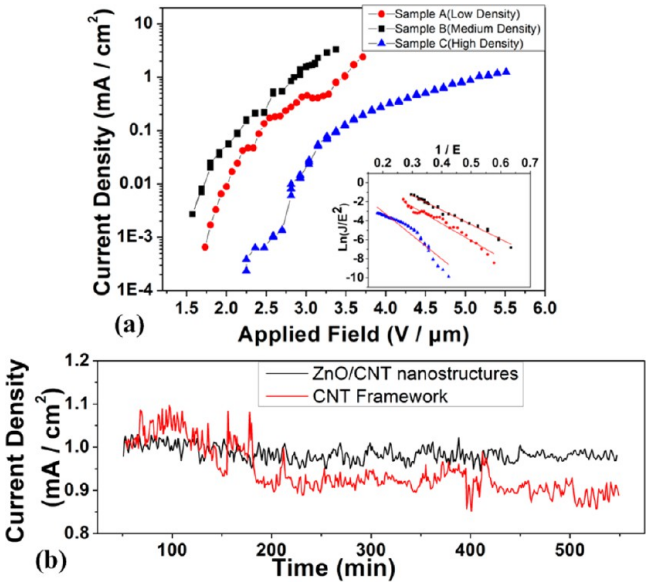

Figure 3. (a) Field emission current density as a function of applied field, and the inserted Fowler–Nordheim plot. (b) Field emission current density as a function of time for ZnO/CNT hierarchical nanostructures (sample B) and pristine CNT framework.

of electric field (J–E curve) with an inset of corresponding F–N plot for the three samples. The threshold electric fields which reach current density of 1 mA/cm^2 are 3.4, 2.8, and 5.1 V/μm for sample A - C, respectively. All the F–N curves exhibit linear dependence which suggests the FE from the emitters obeys a barrier-tunneling process.[18] The value of field enhancement factor β was related to the slop s of F–N curve, and it could be estimated by the equation $\beta = (-B\varphi^{3/2}/s)$. Assuming the work function of ZnO is 5.3 eV, the field enhancement factor β of samples A–C are 3124, 3662, and 2240, respectively. Approximately, β could also be evaluated by the intrinsic morphology parameters of the field emitters.[19] As an hierarchical nanostructure, ZnO/CNT combines the intrinsic geometry of ZnO nanoneedles and CNT framework to obtain an two-step field enhancement β which could be calculated by $\beta = l_{ZnO}l_{CNT}/r$, where l_{ZnO} and l_{CNT} are the lengths of ZnO nanoneedles and CNTs, respectively.[20] r is the tip radius of the ZnO nanoneedle. Therefore, the hierarchical nanostructure leads to an enhanced β of ~4000, which is similar with our experimental measured result. Table 1 tabulates the FE performance of samples in this work and some selected ZnO/CNT hierarchical nanostructures. Clearly, samples in this work shows comparable FE performance with respect to those in the selected literatures. Sample C of high density ZnO nanoneedles suffers from the serious electric field screening provoked by the neighboring field emitters and hence the reduction of FE current. Whereas the best FE performance of sample B is attributed to its medium areal density, which provides more effective emission sites than sample A which has the lowest areal density.

The stability of emission current is one of the most essential characteristics to estimate the FE performance for applications. An accelerated field emission stability test was carried out with relatively higher pressure of 5.0 × 10^{-6} Torr at room

Table 1. Field Emission Performance of the ZnO Nanoneedles on Three-Dimensional CNT Framework in This Work and Some Selected ZnO/CNT Hierarchical Nanostructures

ZnO/CNT hierarchical nanostructures	threshold field at 1 mA/cm^2 (V/μm)	field enhancement factor (β)	ref
ZnO nanowires on CNT fiber	0.70 ± 0.10	41100	21
ZnO nanopins on CNT mat	1.40 ± 0.05	500	12
ZnO nanowires on CNT mesh array	2.30	2000	15
ZnO nanoneedles on CNT framework	2.80–5.1	2240–3662	this work
ZnO nanowires on CNT micropatterns	4.00 ± 0.05	5482	22
ZnO nanoparticles on CNT	4.10	43000	13
ZnO nanoparticles on CNT	5.00	1920	23

temperature. Figure 3b shows the field emission current density as a function of time for ZnO/CNT hierarchical nanostructures (sample B) and pristine CNT framework. The initial field emission current density was set at around 1 mA/cm^2 for two different samples and the applied field was kept constant at 4 V/μm during the test. After 50 mins ageing, the current density of ZnO/CNT hierarchical nanostructures shows no obvious degradation and the corresponding fluctuation is less than 10% which is much stable than that of the CNT framework.

It is worth noting that a good contact of the CNTs with the substrate and the ZnO field emitters is beneficial for improving the FE performance of the devices.[24] Therefore, we studied the current-voltage (I–V) characteristic of the ZnO/CNT field emitters using a simple two-terminal I–V method with gold foil in contact with the top of the field emitters.[25,26] The configuration of the measurement was illustrated in the inset of Figure 4. The resistance of the substrate with Mo electrode

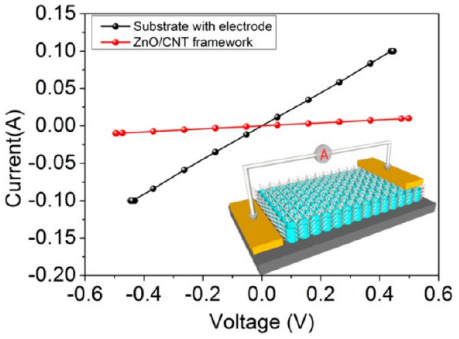

Figure 4. I–V characteristic curves of substrate with Mo electrode and ZnO/CNT hierarchical nanostructures. The inset is the schematic of the two-terminal configuration I–V measurement.

can be calculated to be 4.4 Ω and it rises to 49.7 Ω after growing ZnO/CNT hierarchical nanostructures on it. Since the bandgap of CNT is much narrower than that of ZnO, the junction of ZnO/CNT could be considered as metal–semiconductor junction.[27] Since the existing of a Schottky barrier which could severally limit the current delivery capability at the ZnO/CNT junction, it is critical for CNTs (work function ~5.0 eV) to achieve an Ohmic contact to ZnO

dx.doi.org/10.1021/am402709r | ACS Appl. Mater. Interfaces 2013, 5, 9194–9198

with a higher work function.[28,29] The linear $I-V$ plot in Figure 4 confirms the existing of Ohmic contact between ZnO nanoneedles and CNT framework. During the FE process, the Ohmic ensures the electrons inject from the CNTs can be easily transported into the conduction band of ZnO and finally emitted to the vacuum. The good conductance of electrons prevents excessive high temperature at the heterojunction with high current flow. And, the inherent chemical stability and oxidation resistance also make ZnO stable field emitters in harsh vacuum environments.[30]

To further investigate the effect of the CNT framework in the emission process, we performed electrostatic field simulations by finite element calculation with COMSOL software. Three-dimensional simulation model which represented the pristine CNT microchannel was shown in Figure 5a.

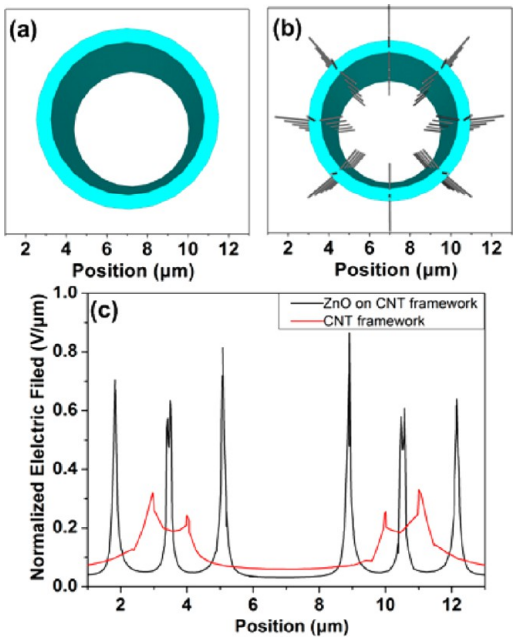

Figure 5. (a) Three-dimensional simulation models of single CNT microchannel and (b) multiple ZnO nanoneedles grown on CNT microchannel. (c) Calculated normalized electric field on the top surface of the field emitters as a function of position.

For comparison, another model (Figure 5b) consists of multiple ZnO nanoneedles grown on CNT microchannel was also employed for simulation. The dimensional parameters of the models were configured according to the SEM images. An electric field of 1 V/μm was applied between the anode and cathode plates. Figure 5c depicted the trends of variation of normalized electric field on the top surface of the models along the path throughout the diameter. The electric field distribution confirmed that the CNT microchannel support the ZnO nanoneedles to obtain a two-step field enhancement at the tips of ZnO nanoneedles, and more emission sites were attributed by the multiple ZnO nanoneedles grown on the three-dimensional CNT microchannel.

CONCLUSIONS

In summary, ZnO nanoneedles with different areal density were synthesized on three-dimensional patterned CNT framework by hydrothermal method. Their FE performances showed strong dependence on the morphology and areal density of ZnO/CNT hierarchical nanostructures. By combining the advantages of high aspect ratio, more effective emission sites with minimized screen effect and good Ohmic contact between ZnO and CNT, the ZnO/CNT hierarchical nanostructures of medium areal density exhibit a low threshold electric field of 2.8 V/μm and a high field enhancement factor of 3662. Its good field emission property makes it promising candidate for cold cathode nanomaterials and its hierarchical morphology is proposed to replace active carbon in the applications of removing toxic dyes in the waste water.[31−33]

AUTHOR INFORMATION

Corresponding Author

*Tel.: +86 25 83792449. Fax: +86 25 83363222. E-mail: chenjingmoon@gmail.com.

Notes

The authors declare no competing financial interest.

ACKNOWLEDGMENTS

The authors gratefully thank the financial supports by the National Key Basic Research Program 973 (2013CB328803, 2010CB327705), the National High-Tech R&D Program 863 of China (2012AA03A302, 2013AA011004), National Natural Science Foundation Project (51002031, 61007036, 61101023, 51202028, and 51120125001), Foundation of Doctoral Program of Ministry of Education Grant (20100092120022, 20120092120025), and the Chinese 111 Project (B07027).

REFERENCES

(1) Li, C.; Lei, W.; Zhang, X. B.; Wang, J. X.; Sun, X. W.; Tan, S. T. *J. Vac. Sci. Technol., B: Microelectron. Nanometer Struct.—Process., Meas., Phenom.* **2007**, *25*, 590−593.
(2) Shang, N. G.; Papakonstantinou, P.; Wang, P.; Zakharov, A.; Palnitkar, U.; Lin, I. N.; Chu, M.; Stamboulis, A. *ACS Nano* **2009**, *3*, 1032−1038.
(3) Ooki, S.; Ohshio, S.; Nishino, J.; Ohkawara, Y.; Ito, H.; Saitoh, H. *Jpn. J. Appl. Phys.* **2008**, *47*, 7303−7307.
(4) Iijima, S.; Ichihashi, T. *Nature* **1993**, *363*, 603−605.
(5) Zhu, M. Y.; Outlaw, R. A.; Bagge-Hansen, M.; Chen, H. J.; Manos, D. M. *Carbon* **2011**, *49*, 2526−2531.
(6) Wang, H. X.; Jiang, N.; Zhang, H.; Hiraki, A. *Carbon* **2010**, *48*, 4483−4488.
(7) Jiang, H.; Hu, J. Q.; Gu, F.; Li, C. Z. *Nanotechnology* **2009**, *20*, 055706.
(8) Zhou, J.; Ding, Y.; Deng, S. Z.; Gong, L.; Xu, N. S.; Wang, Z. L. *Adv. Mater.* **2005**, *17*, 2107.
(9) Hsu, L. C.; Yu, H. C.; Chang, T. H.; Li, Y. Y. *ACS Appl. Mater. Interfaces* **2011**, *3*, 3084−3090.
(10) Wei, Y.; Liu, P.; Jiang, K. L.; Liu, L.; Fan, S. S. *Appl. Phys. Lett.* **2008**, *93*, 023118.
(11) Santini, C. A.; Vereecken, P. M.; Volodin, A.; Groeseneken, G.; De Gendt, S.; Van Haesendonck, C. *Nanotechnology* **2011**, *22*, 395202.
(12) Sugavaneshwar, R. P.; Nagao, T.; Nanda, K. K. *RSC Adv.* **2012**, *2*, 2713−2716.
(13) Ho, Y. M.; Zheng, W. T.; Li, Y. A.; Liu, J. W.; Qi, J. L. *J. Phys. Chem. C* **2008**, *112*, 17702−17708.
(14) Ho, Y. M.; Liu, J. W.; Qi, J. L.; Zheng, W. T. *J. Phys. D: Appl. Phys.* **2008**, *41*, 065308.
(15) Ding, S. Y.; Li, C.; Lei, W.; Zhang, Y.; Qasim, K.; Cui, H. Y.; Zhang, X. B.; Wang, B. P. *Thin Solid Films* **2012**, *524*, 245−248.
(16) Li, C.; Zhang, Y.; Mann, M.; Hasko, D.; Lei, W.; Wang, B. P.; Chu, D. P.; Pribat, D.; Amaratunga, G. A. J.; Milne, W. I. *Appl. Phys. Lett.* **2010**, *97*, 113107.
(17) Maserjian, J.; Zamani, N. *J. Appl. Phys.* **1982**, *53*, 559−567.
(18) Fowler, R. H.; Nordheim, L. *Proc. R. Soc. London, Ser. A* **1928**, *119*, 173−181.

(19) Jo, S. H.; Banerjee, D.; Ren, Z. F. *Appl. Phys. Lett.* **2004**, *85*, 1407−1409.
(20) Stratakis, E.; Giorgi, R.; Barberoglou, M.; Dikonimos, T.; Salernitano, E.; Lisi, N.; Kymakis, E. *Appl. Phys. Lett.* **2010**, *96*, 043110.
(21) Banerjee, D.; Jo, S. H.; Ren, Z. F. *Adv. Mater.* **2004**, *16*, 2028−2032.
(22) Yan, X. B.; Tay, B. K.; Miele, P. *Carbon* **2008**, *46*, 753−758.
(23) Green, J. M.; Dong, L. F.; Gutu, T.; Jiao, J.; Conley, J. F.; Ono, Y. *J. Appl. Phys.* **2006**, *99*, No. 094308.
(24) Chen, H.; Zhang, H. Z.; Fu, L.; Chen, Y.; Williams, J. S.; Yu, C.; Yu, D. P. *Appl. Phys. Lett.* **2008**, *92*, No. 243105.
(25) Yang, D. J.; Wang, S. G.; Zhang, Q.; Sellin, P. J.; Chen, G. *Phys. Lett. A* **2004**, *329*, 207−213.
(26) Jiang, Y. Q.; Wang, P. B.; Lin, L. W. *Nanotechnology* **2011**, *22*, 365704.
(27) Wildoer, J. W. G.; Venema, L. C.; Rinzler, A. G.; Smalley, R. E.; Dekker, C. *Nature* **1998**, *391*, 59−62.
(28) Min, Y. S.; Bae, E. J.; Kim, U. J.; Park, W.; Hwang, C. S. *Appl. Phys. Lett.* **2006**, *89*, No. 113116.
(29) Javey, A.; Guo, J.; Wang, Q.; Lundstrom, M.; Dai, H. *Nature* **2003**, *424*, 654−657.
(30) Li, Q. H.; Wan, Q.; Chen, Y. J.; Wang, T. H.; Jia, H. B.; Yu, D. P. *Appl. Phys. Lett.* **2004**, *85*, 636−638.
(31) Taghizadeh, F.; Ghaedi, M.; Kamali, I.; Sharifpour, E.; Sahraie, R.; Purkait, M. K. *Powder Technol.* **2013**, *245*, 217−226.
(32) Ghaedi, M.; Ghayedi, M.; Kokhdan, S. N.; Sahraei, R.; Daneshfar, A. *J. Ind. Eng. Chem.* **2013**, *19*, 1209−1217.
(33) Ghaedi, M.; Nikman, K.; Zamani, S.; Larki, H.; Roosta, M.; Soylak, M. *Mater. Sci. Eng., C* **2013**, *33*, 3180−3189.